




RESEARCH ARTICLE | MARCH 26 2024

Quantitative assessment of selenium diffusion and passivation in CdSeTe solar cells probed by spatially resolved cathodoluminescence

Bérengère Frouin; Thomas Bidaud; Stefano Pirotta; Tursun Ablekim; John Moseley ; Wyatt K. Metzger; Stéphane Collin  

 Check for updates

APL Mater. 12, 031135 (2024)
<https://doi.org/10.1063/5.0195398>



25 April 2024 21:08:27



APL Quantum
First Articles Online
No Article Processing Charges for Submissions
Through December 31, 2024
[Read Now](#)



Quantitative assessment of selenium diffusion and passivation in CdSeTe solar cells probed by spatially resolved cathodoluminescence

Cite as: APL Mater. 12, 031135 (2024); doi: 10.1063/5.0195398
Submitted: 2 January 2024 • Accepted: 29 February 2024 •
Published Online: 26 March 2024





View Online



Export Citation



CrossMark

Bérengère Frouin,¹ Thomas Bidaud,¹ Stefano Pirota,¹ Tursun Ablekim,² John Moseley,²  Wyatt K. Metzger,² and Stéphane Collin^{1,a)} 

AFFILIATIONS

¹Centre de Nanosciences et de Nanotechnologies, CNRS, Université Paris-Saclay, 91120 Palaiseau, France

²National Renewable Energy Laboratory, Golden, Colorado 80401, USA

^{a)}Author to whom correspondence should be addressed: stephane.collin@c2n.upsaclay.fr

ABSTRACT

The introduction of selenium in CdSeTe/CdTe solar cells has led to improved device performances attributed to the passivation of bulk defects. In this work, high-resolution cathodoluminescence experiments are performed on a series of CdSeTe/CdTe thin films with different Se concentrations to quantify the mechanisms and the passivation role of Se. We demonstrate a universal dependence between the Se concentration and the radiative efficiency and a ten-fold enhancement of the luminescence between CdTe and CdSe_{0.4}Te_{0.6}. Raw luminescence maps are converted into maps of the Se concentration, revealing its graded profile within the stack. We demonstrate the diffusion of Se along CdTe grain boundaries induced by the cadmium chloride annealing treatment and determine the diffusion coefficients, which are more than eight times higher at grain boundaries than in grain interiors. These results provide microscopic insights into the distribution of Se and its impact on the passivation of CdSeTe/CdTe solar cells.

© 2024 Author(s). All article content, except where otherwise noted, is licensed under a Creative Commons Attribution (CC BY) license (<http://creativecommons.org/licenses/by/4.0/>). <https://doi.org/10.1063/5.0195398>

I. INTRODUCTION

Polycrystalline cadmium telluride (CdTe) thin-film solar cells have a very low levelized cost of energy and provide an attractive alternative to silicon technology with a reduced fabrication time and cost. Over the last ten years, CdTe solar cells have benefited from numerous discoveries^{1,2} improving their efficiency from 16.7% to 22.3%.³ However, the efficiency is hindered by the presence of defects in grain interiors (GIs) and at grain boundaries (GBs). The best performances have been obtained by the incorporation of a selenium composition gradient in the CdTe absorber. Se alloy significantly improves the short-circuit current⁴⁻⁷ due to bandgap lowering. Interestingly, the voltage deficit of these devices is maintained or even improved,^{8,9} and excellent optoelectronic properties are reported. The lifetime is increased up to hundreds of nanoseconds for polycrystalline CdSeTe,¹⁰⁻¹² even exceeding 200 ns for devices.¹³ Characterization by cathodoluminescence (CL) sheds light on the passivating role of selenium within the CdTe bulk, with an enhanced

CL signal in the CdSeTe region relative to CdTe.^{11,14} Selenium was shown to diffuse into the CdTe GI/GB mainly along CdSeTe GBs^{15,16} during the CdCl₂ passivation treatment,¹⁷ and experimental evidence of Se reducing harmful non-radiative recombination at grain boundaries has been confirmed.¹⁸ While the mechanism and key role of the Se introduction in CdTe devices have been thoroughly analyzed,^{7,19-21} no quantitative study on the passivation effect of Se has been reported.

In this work, we report on a systematic study on five CdSe_xTe_{1-x} samples with selenium composition ranging from $x = 0$ to $x = 0.4$. The distribution and impact of Se are examined by high-resolution cathodoluminescence (CL) mapping, run under identical conditions for each sample. Using temperature-dependent measurements, we refine the parameters of the Varshni law and the bowing factor of the CdSeTe bandgap, and we convert CL maps into maps of the Se concentration. Hyperspectral CL maps are converted into maps of the Se concentration and are used to quantitatively assess the effects of Se at the nanoscale. We find a correlation between the

luminescence intensity and the Se content, with a ten-fold enhancement of the radiative efficiency between CdTe and CdSe_{0.4}Te_{0.6}. We also determine the diffusion coefficients of Se upon CdCl₂ annealing in grain interiors and at grain boundaries.

II. EXPERIMENTAL DETAILS

A. CdSeTe samples preparation

The cells were fabricated in a superstrate configuration. A soda-lime glass (commercial TEC 12D) was coated with fluorine-doped tin oxide (SnO₂:F) and intrinsic i-SnO₂. Mg_yZnO_{1-y} with $y = 0.08$ was then deposited by radio frequency sputtering using a mixed-oxide target with a weight ratio of 4 and 96 wt. % for MgO and ZnO, respectively. 1 μm of CdSeTe was thermally evaporated from a ternary source of CdSe_xTe_{1-x} at a temperature of 650 °C with a substrate temperature of 450 °C. Five samples with Se compositions ranging from $x = 0$ to $x = 0.4$ by steps of 0.1 were fabricated. Then, without breaking the vacuum, 3–4 μm of CdTe was evaporated, and the samples were CdCl₂-treated at 420 °C for 10 min. Finally, the devices were dipped in a 0.1 mmol CuCl₂ solution in water and annealed in a tube furnace at 200 °C for 30 min in the air. Solar cells were fabricated for each sample and previously studied in Ref. 13.

For CL measurements, 20°-bevels were prepared by focused-ion-beam milling in an xT-Nova NanoLab (FEI Company) with a 30 kV ion beam, followed by surface cleaning with a 5 kV beam [Fig. 1(a)]. Additional cleaning is performed by milling at a glancing angle with Ar⁺ ions using a JEOL cross section polisher tool operating at 3 kV.

B. Characterization

CL measurements were performed in an Attolight Chronos CL-scanning electron microscope (SEM) system. The acceleration voltage of the electron beam was set to 6 keV, and the probe current was kept constant at 4 nA within fluctuations of less than 5%. At 6 kV, Monte Carlo simulation based on the software CASINO shows that 75% and 95% of carriers are generated in CdTe in a pear-shaped excitation volume within a radius/depth of ~25/75 and 85/150 nm, respectively. For CdSe_{0.4}Te_{0.6}, the size of the interaction volume is increased to 40/100 and 110/160 nm, respectively. Luminescence is collected by an achromatic reflective objective designed for constant collection efficiency over a field of view of 150 μm in diameter. Luminescence spectra are dispersed with an Horiba spectrometer iHR320 (diffraction grating with 150 grooves mm⁻¹) and recorded with an Andor Newton charge-coupled device (CCD) camera (1024 × 256 pixels, pixel width 26 μm). The corresponding spectral dispersion is 0.53 nm per pixel. Luminescence spectra are corrected for the diffraction efficiency of the grating and the CCD camera sensitivity. The CL intensity reported in the following corresponds to a spectral density of photon flux per unit of energy (counts s⁻¹ eV⁻¹). The constant excitation and collection efficiencies during the experiments guarantee a quantitative comparison between the different samples.

To analyze the chemical composition of the samples, energy dispersive spectroscopy (EDS) measurements are operated with an acceleration voltage of 6 keV in a Zeiss Merlin VP SEM. Transmission electron microscopy (TEM) images were acquired at 200 kV on the sample CdSe_{0.2}Te_{0.8}. The system, equipped with an energy

dispersive x-ray (EDX) detector, was used to investigate elemental distribution maps along the lamella.

III. CATHODOLUMINESCENCE EXPERIMENTS

A. CL maps of CdSeTe/CdTe thin films

The CL panchromatic maps measured on the bevels at room temperature are plotted in Figs. 1(b) and 1(e)–1(h). They show the evolution of the grain morphology and the luminescence intensity across the depth of each CdSeTe/CdTe thin film. The grayscale is adjusted for each sample to account for the strong differences in the luminescence intensities. In Figs. 1(e)–1(h), there is a clear contrast between the top and the bottom of the CL intensity maps, revealing the bilayer structure where the CdTe region can be distinguished from the CdSeTe. The CdSeTe region (bottom of CL maps) exhibits smaller grains as compared to the top CdTe area. Contrary to previous CL studies of pure CdTe thin films²² we see no obvious correlation between the CL intensity and the grain size. On the other hand, we observe a strong increase in the luminescence intensity with the Se concentration, with a ten-fold enhancement between CdTe [Fig. 1(a)] and CdSe_{0.4}Te_{0.6} [Fig. 1(h)]. A similar CL intensity contrast between regions with high and low Se contents has already been observed by Fiducia *et al.* in a single CdSeTe/CdTe bi-layer and attributed to the passivation effect of selenium.¹⁴

Normalized CL spectra averaged over the homogeneous CdSeTe area, highlighted with a colored rectangle on all the panchromatic maps, are shown in Fig. 1(d). These data can be fitted with the generalized Planck law, as described in the supplementary material (Sec. I). The resulting fits are in very good agreement with the experimental data. The absorption coefficient is modeled by a parabolic band approximation convoluted with an exponential decay below the bandgap to account for the Urbach tail. A Gaussian function is used to model the low-energy emission peak attributed to a defect level. The main fitted parameters are reported in Table I. We note that the bandgap is 10–15 meV below the main peak energy. The defect level is found 120–180 meV below the bandgap, with the energy difference increasing with Se concentration. It is also clearly seen in low-temperature CL spectra. It is usually attributed to A-center defects induced by complexes formed between cadmium vacancies and shallow donors.^{23–28} Aside from the $x = 0.3$ sample, the bandtail slightly increases with the Se content, from 10.5 meV for CdTe to 12.2 meV for CdSe_{0.4}Te_{0.6} (see the supplementary material, Table I), whereas the V_{oc} deficit with respect to the Shockley–Queisser limit decreases from about 630 to 330 mV correspondingly.¹³ In this case, the simplistic relationship between V_{oc} and the Urbach bandtail suggested by Wolter *et al.* does not hold.²⁹

The peak energy of luminescence spectra is also extracted for each pixel of the hyperspectral CL maps and plotted as peak energy maps in Figs. 1(c) and 1(i)–1(l). It provides a direct insight into the variation in the selenium concentration. As expected, the peak energy map of the pure CdTe sample [Fig. 1(c)] is homogeneous over the entire depth. For the other samples, the luminescence redshifts as the selenium concentration increases. In Figs. 1(i)–1(l), the peak energy maps exhibit two distinct and homogeneous areas corresponding to CdTe (top) with a peak energy of around 1.51 eV, and to CdSeTe (bottom) with peak energies from 1.47 to 1.41 eV. Moreover, a steep transition between the CdTe and CdSeTe is

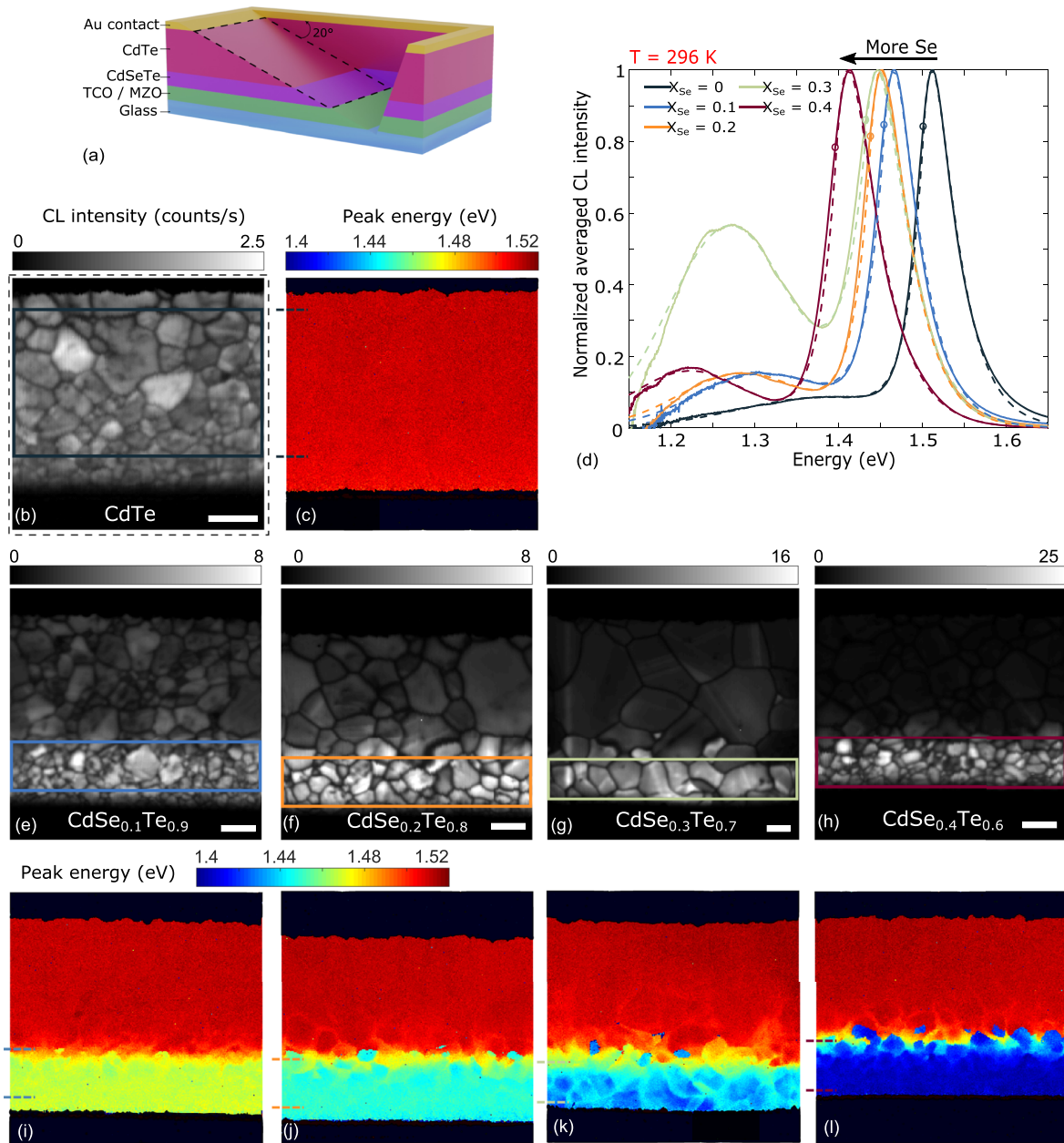


FIG. 1. (a) Schematic of a beveled CdSeTe/CdTe sample, the black dashed rectangle indicates the CL measurement region. (b) and (e)–(h) Room-temperature panchromatic CL maps (256×256 pixels) of $\text{CdSe}_x\text{Te}_{1-x}$ samples with compositional x values of (b) $x = 0$, (e) $x = 0.1$, (f) $x = 0.2$, (g) $x = 0.3$, and (h) $x = 0.4$. The grayscale bars are adjusted for each CL intensity map. The white scale bar stands for $3 \mu\text{m}$. (c) and (i)–(l) Corresponding CL peak energy maps of (c) $x = 0$, (i) $x = 0.1$, (j) $x = 0.2$, (k) $x = 0.3$, and (l) $x = 0.4$. (d) Normalized CL spectra averaged over the homogeneous area shown as a colored rectangle at 296 K for the five samples. The dotted lines correspond to the generalized Planck law fit, and the open circles on the CL spectra indicate the bandgaps determined from the fit.

observed, and small inhomogeneities along the grain structure are revealed. We note that the $\text{CdSe}_{0.3}\text{Te}_{0.7}$ sample differs from the others with bigger grains and a less homogeneous CdSeTe region [Fig. 1(k)].

The region of high luminescence on the panchromatic maps consistently aligns with the CdSeTe region, irrespective of the nominal bulk concentration of selenium. In Sec. IV, we will quantify the relationship between luminescence intensity and selenium concen-

25 April 2024 21:08:27

tration. Then, in Sec. V, the analysis will be expanded to examine the spatial distribution of selenium within the CdTe layer as well as the underlying selenium diffusion mechanisms.

IV. IMPACT OF Se CONCENTRATION ON RADIATIVE EFFICIENCY

The beneficial impact of the selenium concentration on the radiative efficiency can be seen in Fig. 2. We extracted the energy and the intensity of the main emission peak from each pixel of the four hyperspectral CL maps recorded on the CdSeTe/CdTe samples. The values are sorted by peak energy in 0.6 meV intervals, and the average CL intensity of the main peak is computed within each interval. Figure 2 shows a rise in luminescence efficiency as the peak energy decreases. Two striking features are visible. First, the data from different samples are superimposed. It means that the same luminescence intensity is found for the same Se concentration in the four samples, despite the different nominal concentrations and diffusion processes. Second, the data show a ten-fold increase between CdTe (1.50 eV) and CdSe_{0.4}Te_{0.6} (1.4 eV). The relationship between the CL intensity and the peak energy can be fitted with a phenomenological exponential law,

$$I_{CL}(E) = a \cdot \exp(-E/b), \quad (1)$$

where $b = 53$ meV.

These results demonstrate the direct relationship between the Se content and the radiative efficiency. Regardless of the sample, grain size, or position on the bevel, the CL peak intensity is determined by the local Se concentration.

What is the impact of the enhanced radiative efficiency on the quasi-Fermi level splitting $\Delta\mu$ and open-circuit voltage? The absorption coefficient of CdSeTe is spectrally shifted with the bandgap but with little change in its spectral shape (see the supplementary material, Sec. I). As a result, the luminescence intensity at the peak energy E_{peak} is mainly driven by a factor $E_{peak}^2 \exp[-(E_{peak} - \Delta\mu)/kT]$,^{30–32} where the exponential term dominates. From $x_{Se} = 0$ to $x_{Se} = 0.4$, the decrease in the quasi-Fermi level splitting induced by the bandgap lowering of about 100 meV is partly counterbalanced by the increase in the radiative efficiency, which accounts for about 60 meV. Overall, this effect can partly but not fully explain the

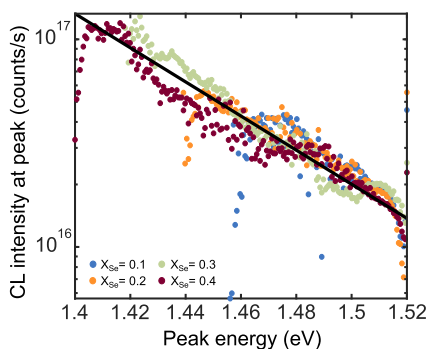


FIG. 2. Room-temperature CL intensity as a function of the CL peak position combined from the four CdSe_xTe_{1-x} samples with Se content ranging from 0.1 to 0.4. The mean CL intensity is calculated for each energy range and sample.

increase in open-circuit voltage beyond 200 mV measured for the same set of samples.¹³

V. GRADIENT OF Se

We have performed a series of experiments and proposed a set of equations to determine the bandgap $E_g(T, x_{Se})$ of CdSeTe semiconductor alloys for any concentration $x_{Se} < 0.4$ and temperature between 0 and 300 K (see the supplementary material). We extracted the bandgap from hyperspectral maps performed at nine different temperatures for the five samples. From this dataset, we have refined the parameters of the Varshni law [Eq. (3)] and the bowing factor of the CdSeTe bandgap [Eq. (2)]. As a result, the following equations provide the relationship between the bandgap, the temperature, and the selenium composition:

$$E_g(0, x_{Se}) = 1.589(1 - x_{Se}) + 1.75x_{Se} - 0.67x_{Se}(1 - x_{Se}), \quad (2)$$

$$E_g(T, x_{Se}) = E_g(0, x_{Se}) - \frac{5 \times 10^{-4} T^2}{T + 200}. \quad (3)$$

In the following, we use these equations to convert the peak energy maps into Se concentration maps at 296 K.

A. Gradient of Se concentration in the depth

The exact distribution of Se content is calculated at room temperature, and with a 10 meV shift between the peak energy (E_{peak}) and the bandgap, we obtain for $x_{Se} < 0.4$,

$$E_{peak}(x_{Se}) = 1.51(1 - x_{Se}) + 1.67x_{Se} - 0.67x_{Se}(1 - x_{Se}). \quad (4)$$

Maps of the Se concentration are plotted in Figs. 3(a)–3(c), where the common colorscale highlights the global increase in Se content between the samples. Due to the band bowing of CdSeTe compounds, the bandgap is nearly constant around $x_{Se} = 0.4$, and the map of Se concentration cannot be extracted accurately for the CdSe_{0.4}Te_{0.6} sample. The Se content was also determined in homogeneous regions by SEM/EDS, and by STEM/EDS (the supplementary material, Fig. 4) for the sample CdSe_{0.2}Te_{0.8}. The values obtained by EDS are less accurate but confirm the trends found in the maps of the Se concentration. For a nominal Se content of 0.1, we find an average of $x_{Se} = 9\%$ in the CdSeTe region of CL maps, confirmed by the 12% found by SEM/EDS. For a nominal Se content of 0.2, a selenium concentration lower than expected is found, with an average of 14%–15% in the CL map, corroborated by an estimation of 17% by SEM/EDS and 10%–14% by STEM/EDS. The CdSeTe region of the CdSe_{0.3}Te_{0.7} sample is more heterogeneous, with an average x_{Se} of around 20% for both CL and SEM/EDS estimation and a higher concentration exhibited locally in the CL map [Fig. 3(c)]. Overall, the absolute value of x_{Se} is difficult to estimate precisely, but the high spectral resolution of CL maps translates into an estimation of x_{Se} with an accuracy of less than 0.5% for low Se concentrations, and can be used to study the diffusion of selenium at the nanoscale.

These maps exhibit concentration inhomogeneities at the grain level in the interdiffusion region. In the CdTe region, a small concentration of Se (about 1%) is found at the grain boundaries. It could be the signature of higher diffusion coefficients of Se at grain boundaries as compared to grain interiors, with a potential impact on the transport and passivation properties.

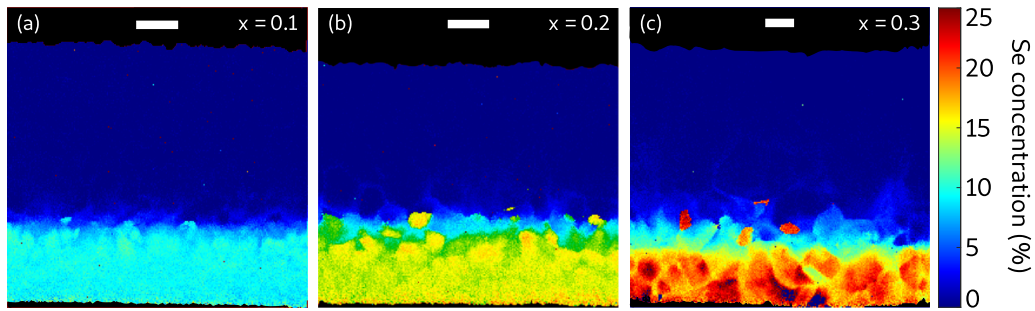


FIG. 3. (a)–(c) Maps of the Se concentration x_{Se} extracted from the CL maps of the peak energy [Figs. 1(i)–1(k)] and Eq. (4) for nominal compositions of the CdSeTe region of (a) $x = 0.1$, (b) $x = 0.2$ and, (c) $x = 0.3$. White scale bar: $3 \mu\text{m}$.

B. Se diffusion along grain boundaries

Selenium diffusion is mainly driven by the CdCl_2 annealing and appears to be favored along GBs.^{14,17,18} In the following, we use the Se concentration maps to quantify the gradients of composition in the vicinity of the interdiffusion region, both in grain interiors and at grain boundaries, and we assess the diffusion coefficients of Se in CdTe. We illustrate this analysis for the $\text{CdSe}_{0.2}\text{Te}_{0.8}$ sample in

Fig. 4. The map of x_{Se} exhibits a clear increase in the Se concentration in the GBs of CdTe close to the interdiffusion region [Fig. 4(b)]. Figure 4(c) shows an increase of 1% across a GB. In-depth profiles of x_{Se} have been extracted from different linescans [colored lines in Fig. 4(a)], in order to investigate the decrease in the Se concentration away from the Se-rich region, in grain interiors [Fig. 4(d)], along GBs [Fig. 4(e)], and along a straight line [Fig. 4(f)]. The signal is

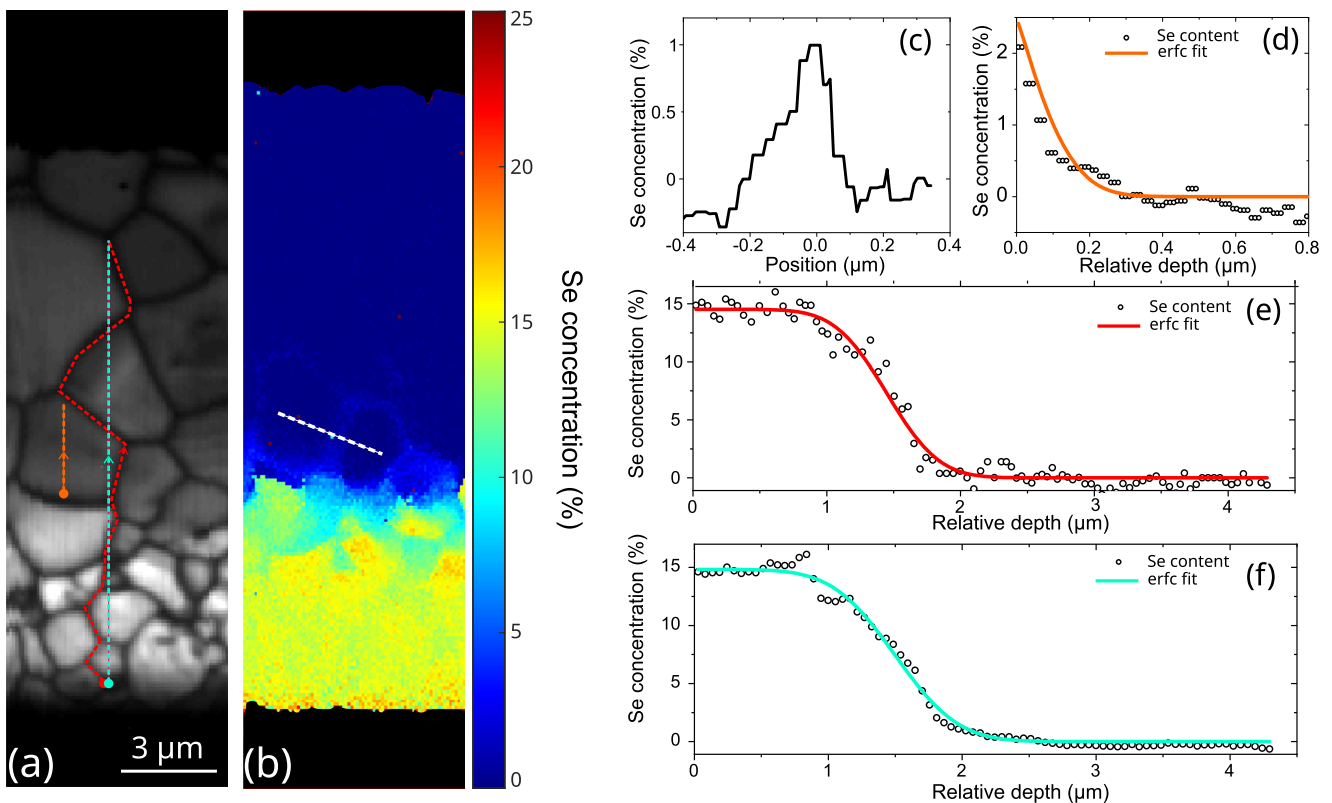


FIG. 4. (a) RT panchromatic map of $\text{CdSe}_{0.2}\text{Te}_{0.8}$, where the analyzed line profiles are indicated by the colored dotted lines. (b) Corresponding Se concentration map emphasizing a higher Se content in GB. (c) Se concentration profile across one of the grain boundaries [white dotted line in (b)]. (d)–(f) Data and fits of selenium concentration in-depth profiles. The color of the fit matches the indicated lines in (a). The colored dots and the arrows in panel (a) indicate the origin and the positive direction along the linescan, respectively. The relative depth in (d)–(f) corresponds to the vertical position of pixels in the layer.

integrated over a width of 250 nm, and the pixel position is translated into the depth z .

The profiles are fitted with a 1D diffusion model³³ that assumes a constant reservoir of Se at the CdSeTe/CdTe interface, and we determine the diffusion coefficient D of Se atoms during the annealing process performed at 420 °C during $t = 10$ min,

$$C(t, z) = \frac{C_0}{2} \operatorname{erfc}\left(\frac{z-h}{2\sqrt{Dt}}\right), \quad (5)$$

where erfc is the complementary error function.

For the intragrain diffusion [Fig. 4(d)], care was taken to extract a profile perpendicular to the interface in a large grain. A bulk diffusion coefficient of $D = 1.2 \times 10^{-13}$ cm²/s is found. The same fitting procedure leads to a diffusion coefficient six times larger along grain boundaries, $D = 7.8 \times 10^{-13}$ cm²/s [Fig. 4(e)]. This result confirms that the diffusion of Se is mainly driven by grain boundaries, and provides a quantification of the mechanism. The use of a straight linescan across the depth of the CdTe layer is a simpler way to extract profiles of x_{Se} [Fig. 4(f)] and results in $D = 1.1 \times 10^{-12}$ cm²/s, close to the value for GBs.

The same analysis was performed on straight linescans for each sample with nominal compositional values of $x = 0.1, 0.2$, and 0.3 in three distinct areas. The results of the diffusion coefficient are reported in the supplementary material (Table IV and Fig. 5). D increases with the concentration of Se in the CdSeTe reservoir, from $D = 0.5 \times 10^{-12}$ cm²/s for $x = 0.1$ to $D = 5 \times 10^{-12}$ cm²/s for $x = 0.3$.

VI. CONCLUSION

Quantitative assessment of the selenium diffusion and passivation mechanisms in CdSeTe was performed using highly resolved cathodoluminescence maps. This systematic study with different selenium contents has shown a strong correlation between the luminescence intensity and the selenium concentration, with a common behavior for all samples. The radiative efficiency can be expressed as a function of the Se concentration with a phenomenological law and exhibits a ten-fold increase between CdTe and CdSe_{0.4}Te_{0.6}. Using temperature-dependent CL maps, we have refined the parameters of the Varshni law and the bowing factors, leading to a relationship between the bandgap, the temperature, and the Se concentration. It is used to convert hyperspectral CL maps into maps of the Se concentration. Therefore, CL maps provide nanoscale information on the selenium distribution in a non-destructive manner and enable the quantification of the Se atom diffusion coefficient both in grain interiors and at grain boundaries.

Various fabrication processes have been investigated recently for the deposition of CdSeTe layers with composition gradients.^{34–36} Our results could guide the development of such processes based on sequential deposition and annealing. They also give important information about the Se profile in CdTe solar cells, which can be used for more accurate device simulation. These results demonstrate the potential of cathodoluminescence to map the optoelectronic properties of polycrystalline semiconductors and to link the radiative efficiency to the composition of alloys at the nanoscale.

SUPPLEMENTARY MATERIAL

Additional information includes the determination of the bandgap and Urbach tail of CdSeTe material, the determination of the selenium and temperature dependence of the bandgap, and details on the gradient and diffusion coefficient of selenium in the CdSeTe/CdTe layers.

ACKNOWLEDGMENTS

The authors thank Ludovic Largeau for EDS measurements and Joel N. Duenow, Xin Zheng, and Eric Colegrove for their contribution to sample preparation. The authors acknowledge the support of the French RENATECH network. This work was authored in part by the National Renewable Energy Laboratory, operated by Alliance for Sustainable Energy, LLC, for the U.S. Department of Energy (DOE) under Contract No. DE-AC36-08GO28308. The funding was provided by the U.S. Department of Energy Office of Energy Efficiency and Renewable Energy Solar Energy Technologies Office and Grant No. CRD-13-507. The views expressed in the article do not necessarily represent the views of the DOE or the U.S. Government.

AUTHOR DECLARATIONS

Conflict of Interest

The authors have no conflicts to disclose.

Author Contributions

Béregère Frouin: Formal analysis (equal); Investigation (equal); Methodology (equal); Writing – original draft (equal); Writing – review & editing (equal). **Thomas Bidaud:** Formal analysis (equal); Methodology (equal); Writing – review & editing (equal). **Stefano Pirotta:** Formal analysis (equal); Writing – review & editing (equal). **Tursun Ablekim:** Investigation (equal); Writing – review & editing (equal). **John Moseley:** Formal analysis (equal); Investigation (equal); Methodology (equal); Writing – review & editing (equal). **Wyatt K. Metzger:** Investigation (equal); Writing – review & editing (equal). **Stéphane Collin:** Conceptualization (equal); Formal analysis (equal); Funding acquisition (equal); Methodology (equal); Project administration (equal); Supervision (equal); Writing – original draft (equal); Writing – review & editing (equal).

DATA AVAILABILITY

The data that support the findings of this study are available from the corresponding author upon reasonable request.

REFERENCES

- 1T. Ablekim, J. N. Duenow, X. Zheng, H. Moutinho, J. Moseley, C. L. Perkins, S. W. Johnston, P. O'Keefe, E. Colegrove, D. S. Albin, M. O. Reese, and W. K. Metzger, "Thin-film solar cells with 19% efficiency by thermal evaporation of CdSe and CdTe," *ACS Energy Lett.* **5**, 892–896 (2020).
- 2W. K. Metzger, S. Grover, D. Lu, E. Colegrove, J. Moseley, C. L. Perkins, X. Li, R. Mallick, W. Zhang, R. Malik, J. Kephart, C. S. Jiang, D. Kuciauskas, D. S. Albin,

- M. M. Al-Jassim, G. Xiong, and M. Gloeckler, "Exceeding 20% efficiency with in situ group V doping in polycrystalline CdTe solar cells," *Nat. Energy* **4**, 837–845 (2019).
- ³R. Mallick, X. Li, C. Reich, X. Shan, W. Zhang, T. Nagle, L. Bok, E. Bicakci, N. Rosenblatt, D. Modi, R. Farshchi, C. Lee, J. Hack, S. Grover, N. Wolf, W. Metzger, D. Lu, and G. Xiong, "Arsenic-doped CdSeTe solar cells achieve world record 22.3% efficiency," *IEEE J. Photovolt.* **13**, 510–515 (2023).
- ⁴N. R. Paudel and Y. Yan, "Enhancing the photo-currents of CdTe thin-film solar cells in both short and long wavelength regions," *Appl. Phys. Lett.* **105**, 183510 (2014).
- ⁵A. Munshi, J. Kephart, A. Abbas, J. Raguse, J.-N. Beaudry, K. Barth, J. Sites, J. Walls, and W. Sampath, "Polycrystalline CdSeTe/CdTe absorber cells with 28 mA/cm² short-circuit current," *IEEE J. Photovolt.* **8**, 310–314 (2018).
- ⁶J. Guo, A. Mannodi-Kanakkithodi, F. G. Sen, E. Schwenker, E. S. Barnard, A. Munshi, W. Sampath, M. K. Chan, and R. F. Klie, "Effect of selenium and chlorine co-passivation in polycrystalline CdSeTe devices," *Appl. Phys. Lett.* **115**, 153901 (2019).
- ⁷J. D. Poplawsky, W. Guo, N. Paudel, A. Ng, K. More, D. Leonard, and Y. Yan, "Structural and compositional dependence of the CdTe_xSe_{1-x} alloy layer photoactivity in CdTe-based solar cells," *Nat. Commun.* **7**, 12537 (2016).
- ⁸A. Onno, C. Reich, S. Li, A. Danielson, W. Weigand, A. Bothwell, S. Grover, J. Bailey, G. Xiong, D. Kuciauskas, W. Sampath, and Z. C. Holman, "Understanding what limits the voltage of polycrystalline CdSeTe solar cells," *Nat. Energy* **7**, 400 (2022).
- ⁹A. M. Bothwell, J. A. Drayton, P. M. Jundt, and J. R. Sites, "Characterization of thin CdTe solar cells with a CdSeTe front layer," *MRS Adv.* **4**, 2053–2062 (2019).
- ¹⁰D. B. Li, C. Yao, S. N. Vijayaraghavan, R. A. Awani, K. K. Subedi, R. J. Ellingson, L. Li, Y. Yan, and F. Yan, "Low-temperature and effective ex situ group V doping for efficient polycrystalline CdSeTe solar cells," *Nat. Energy* **6**, 715–722 (2021).
- ¹¹X. Zheng, D. Kuciauskas, J. Moseley, E. Colegrove, D. S. Albin, H. Moutinho, J. N. Duenow, T. Ablekim, S. P. Harvey, A. Ferguson, and W. K. Metzger, "Recombination and bandgap engineering in CdSeTe/CdTe solar cells," *APL Mater.* **7**, 71112 (2019).
- ¹²D. Kuciauskas, J. Moseley, P. Ščajev, and D. Albin, "Radiative efficiency and charge-carrier lifetimes and diffusion length in polycrystalline CdSeTe heterostructures," *Phys. Status Solidi RRL* **14**, 1900606 (2020).
- ¹³T. Ablekim, J. N. Duenow, C. L. Perkins, J. Moseley, X. Zheng, T. Bidaud, B. Frouin, S. Collin, M. O. Reese, M. Amarasinghe, E. Colegrove, S. Johnston, and W. K. Metzger, "Exceeding 200 ns lifetimes in polycrystalline CdTe solar cells," *Sol. RRL* **5**, 2100173 (2021).
- ¹⁴T. A. M. Fiducia, B. G. Mendis, K. Li, C. R. M. Grovenor, A. H. Munshi, K. Barth, W. S. Sampath, L. D. Wright, A. Abbas, J. W. Bowers, and J. M. Walls, "Understanding the role of selenium in defect passivation for highly efficient selenium-alloyed cadmium telluride solar cells," *Nat. Energy* **4**, 504–511 (2019).
- ¹⁵T. A. Fiducia, K. Li, A. H. Munshi, K. Barth, W. S. Sampath, C. R. Grovenor, and J. M. Walls, "Three-dimensional imaging of selenium and chlorine distributions in highly efficient selenium-graded cadmium telluride solar cells," *IEEE J. Photovolt.* **10**, 685–689 (2020).
- ¹⁶A. Shah, A. P. Nicholson, T. A. M. Fiducia, A. Abbas, R. Pandey, J. Liu, C. Grovenor, J. M. Walls, W. S. Sampath, and A. H. Munshi, "Understanding the copassivation effect of Cl and Se for CdTe grain boundaries," *ACS Appl. Mater. Interfaces* **13**, 35086–35096 (2021).
- ¹⁷A. H. Munshi, J. M. Kephart, A. Abbas, A. Danielson, G. Gelinas, J. N. Beaudry, K. L. Barth, J. M. Walls, and W. S. Sampath, "Effect of CdCl₂ passivation treatment on microstructure and performance of CdSeTe/CdTe thin-film photovoltaic devices," *Sol. Energy Mater. Sol. Cells* **186**, 259–265 (2018).
- ¹⁸T. Fiducia, A. Howkins, A. Abbas, B. Mendis, A. Munshi, K. Barth, W. Sampath, and J. Walls, "Selenium passivates grain boundaries in alloyed CdTe solar cells," *Sol. Energy Mater. Sol. Cells* **238**, 111595 (2022).
- ¹⁹E. Artegiani, A. Gasparotto, M. Meneghini, G. Meneghesso, and A. Romeo, "How the selenium distribution in CdTe affects the carrier properties of CdSeTe/CdTe solar cells," *Sol. Energy* **260**, 11–16 (2023).
- ²⁰M. Amarasinghe, D. Albin, D. Kuciauskas, J. Moseley, C. L. Perkins, and W. K. Metzger, "Mechanisms for long carrier lifetime in Cd(Se)Te double heterostructures," *Appl. Phys. Lett.* **118**, 211102 (2021).
- ²¹M. J. Watts, T. A. M. Fiducia, B. Sanyal, R. Smith, J. M. Walls, and P. Goddard, "Enhancement of photovoltaic efficiency in CdSe_xTe_{1-x} (where 0 ≤ x ≤ 1): Insights from density functional theory," *J. Phys.: Condens. Matter* **32**, 125702 (2020).
- ²²J. Moseley, P. Rale, S. Collin, E. Colegrove, H. Guthrey, D. Kuciauskas, H. Moutinho, M. Al-Jassim, and W. K. Metzger, "Luminescence methodology to determine grain-boundary, grain-interior, and surface recombination in thin-film solar cells," *J. Appl. Phys.* **124**, 113104 (2018).
- ²³V. Consonni, G. Feuillet, and S. Renet, "Spectroscopic analysis of defects in chlorine doped polycrystalline CdTe," *J. Appl. Phys.* **99**, 053502 (2006).
- ²⁴N. C. Giles-Taylor, R. N. Bicknell, D. K. Blanks, T. H. Myers, and J. F. Schetzina, "Photoluminescence of CdTe: A comparison of bulk and epitaxial material," *J. Vac. Sci. Technol., A* **3**, 76–82 (1985).
- ²⁵D. P. Halliday, J. M. Eggleston, and K. Durose, "A photoluminescence study of polycrystalline thin-film CdTe/CdS solar cells," *J. Cryst. Growth* **186**, 543–549 (1998).
- ²⁶J. Krustok, V. Valdna, K. Hjelt, and H. Collan, "Deep center luminescence in p-type CdTe," *J. Appl. Phys.* **80**, 1757–1762 (1996).
- ²⁷C. Kraft, H. Metzner, M. Hädrich, U. Reislöhner, P. Schley, G. Gobsch, and R. Goldhahn, "Comprehensive photoluminescence study of chlorine activated polycrystalline cadmium telluride layers," *J. Appl. Phys.* **108**, 124503 (2010).
- ²⁸T. Bidaud, J. Moseley, M. Amarasinghe, M. Al-Jassim, W. K. Metzger, and S. Collin, "Imaging CdCl₂ defect passivation and formation in polycrystalline CdTe films by cathodoluminescence," *Phys. Rev. Mater.* **5**, 064601 (2021).
- ²⁹M. H. Wolter, R. Carron, E. Avancini, B. Bissig, T. P. Weiss, S. Nishiwaki, T. Feuer, S. Buecheler, P. Jackson, W. Witte, and S. Siebentritt, "How band tail recombination influences the open-circuit voltage of solar cells," *Prog. Photovolt.: Res. Appl.* **30**, 702–712 (2022).
- ³⁰J. K. Katahara and H. W. Hillhouse, "Quasi-fermi level splitting and sub-bandgap absorptivity from semiconductor photoluminescence," *J. Appl. Phys.* **116**, 173504 (2014).
- ³¹J. K. Katahara and H. W. Hillhouse, "Erratum: "quasi-fermi level splitting and sub-bandgap absorptivity from semiconductor photoluminescence" [J. Appl. Phys. **116**, 173504 (2014)]," *J. Appl. Phys.* **119**, 239901 (2016).
- ³²P. Würfel and U. Würfel, *Physics of Solar Cells: From Basic Principles to Advanced Concepts* (John Wiley & Sons, Ltd., 2016).
- ³³E. Colegrove, X. Zheng, T. Ablekim, J. N. Duenow, C. L. Perkins, H. R. Moutinho, and W. K. Metzger, "Se diffusion in CdTe thin films for photovoltaics," *J. Phys.: D: Appl. Phys.* **54**, 025501 (2021).
- ³⁴O. Oklobia, G. Kartopu, S. Jones, P. Siderfin, B. Grew, H. K. Lee, W. C. Tsoi, A. Abbas, J. M. Walls, D. L. McGott, M. O. Reese, and S. J. Irvine, "Development of arsenic doped Cd(Se, Te) absorbers by MOCVD for thin film solar cells," *Sol. Energy Mater. Sol. Cells* **231**, 111325 (2021).
- ³⁵E. Artegiani, A. Gasparotto, P. Punathil, V. Kumar, M. Barbato, M. Meneghini, G. Meneghesso, F. Piccinelli, and A. Romeo, "A new method for CdSe_xTe_{1-x} band grading for high efficiency thin-absorber CdTe solar cells," *Sol. Energy Mater. Sol. Cells* **226**, 111081 (2021).
- ³⁶A. Romeo and E. Artegiani, "CdTe-based thin film solar cells: Past, present and future," *Energies* **14**, 1684 (2021).